bioRxiv preprint doi: https://doi.org/10.1101/2022.03.22.485353; this version posted March 25, 2022. The copyright holder for this preprint (which was not certified by peer review) is the author/funder. All rights reserved. No reuse allowed without permission.

Intrathecal tracer dispersion is accelerated by high volume injection and natural micromixing

Ayankola O. Ayansiji[1], Daniel S. Gehrke[1], Bastien Baralle[1,2], Ariel Nozain[1,2], and Andreas A. Linninger[1,3*]

[1] Department of Bioengineering, University of Illinois at Chicago, Chicago, Illinois, USA.

[2] UIC student intern from EPF, Ecole D'Ingénieur, Paris, France.

[3] Department of Neurosurgery, University of Illinois at Chicago, Chicago, Illinois, USA.

Corresponding author:

Andreas A. Linninger, Department of Biomedical Engineering and Neurosurgery, University of Illinois at Chicago, Chicago, IL, USA.

Email: linninge@uic.edu

Phone (office): 312-4137743

Running Head:

Prediction of intrathecal drug administration

bioRxiv preprint doi: https://doi.org/10.1101/2022.03.22.485353; this version posted March 25, 2022. The copyright holder for this preprint (which was not certified by peer review) is the author/funder. All rights reserved. No reuse allowed without permission.

Abstract

Background

Traditionally, there is a widely held belief that drug dispersion after intrathecal (IT) delivery is confined to a small location near the injection site. We posit that high volume infusions can overcome this perceived limitation of IT administration.

Methods

To test our hypothesis, subject-specific deformable phantom models of the human central nervous system were manufactured so that tracer infusion could be realistically replicated in vitro over the entire physiological range of pulsating cerebrospinal fluid (CSF) amplitudes and frequencies. Dispersion of IT injected tracers was studied systematically with high-speed optical methods to determine the relative impact of injection parameters including infusion volume, flow rate and catheter configurations and natural CSF oscillations.

Results

Optical imaging analysis of high-volume infusion experiments showed that tracer disperses quickly throughout the spinal subarachnoid space (SAS) reaching the cervical region in less than ten minutes; this is much faster than suggested by prior theories (Taylor-Aris-Watson dispersion). Our experiments indicate that micro-mixing patterns induced by oscillatory CSF flow around microanatomical features such as nerve roots significantly accelerate solute dispersion. Strong micro mixing effects caused by anatomical features in the spinal subarachnoid space are present in intrathecal drug administration, but were not considered in prior dispersion theories, which explains why prior models developed in the engineering community are poor predictors for IT delivery.

bioRxiv preprint doi: https://doi.org/10.1101/2022.03.22.485353; this version posted March 25, 2022. The copyright holder for this preprint (which was not certified by peer review) is the author/funder. All rights reserved. No reuse allowed without permission.

Conclusion

Our experiments support the feasibility of targeting large sections of the neuroaxis or brain by means of high-volume injection protocols. The experimental tracer dispersion profiles acquired with an in vitro human CNS analog informed a new predictive model of tracer dispersion as a function of physiological CSF pulsations and adjustable infusion parameters. The ability to predict spatiotemporal dispersion patterns is an essential prerequisite for exploring new indications of IT drug delivery which target specific regions in the central nervous system (CNS) or the brain.

Keywords*:* Geometry Induced Mixing, Intrathecal Drug Delivery, Method of Moments, Oscillatory Flow, In vitro Spine Model, Drug Infusion Parameters.

Background

Early studies on intrathecal (IT) administration in pigs using very low infusion rates [1] contributed to the widely held belief that IT administration is confined to a small location near the injection site and thus is unsuitable for drug targeting of the brain. This notion enjoys theoretical support from the conjecture that IT drug delivery follows the well-known phenomenon of Taylor dispersion of solutes in oscillatory pipe flow [2], [3]. However, the applicability of Taylor dispersion on drug transport in oscillatory CSF flow has not been tested in vivo due to technical difficulties and risk to patients. Tracking tracer dispersion in vivo with multimodal PET/MRI [4] or computed tomography angiography suffer limitations in spatial and temporal feature resolution [5]. Especially, observation of fast injection jets would require real-time acquisition rates unavailable in current non-invasive imaging technology [6]. Hence, technical limitations for tracking solutes suspended in complex CSF flow and patient safety make in vivo quantification problematic, if not impractical. In vitro experiments using an anatomically accurate model of the spinal subarachnoid space (SAS) are a compliment and a logical alternative to authentic, but often

bioRxiv preprint doi: https://doi.org/10.1101/2022.03.22.485353; this version posted March 25, 2022. The copyright holder for this preprint (which was not certified by peer review) is the author/funder. All rights reserved. No reuse allowed without permission.

inaccurate in vivo infusion trials with limited temporal and spatial resolution. Several labs have also employed in vitro models for studying CNS dynamics [7]–[10]. IT *bench top testing* with optical image analysis offers the distinct advantage of high temporal and spatial resolution, which is necessary for systematic parameter studies of the correlation between infusion and physiological parameters (=anatomy and CSF dynamics) and achievable drug dispersion. A key requirement for the validity of infusion bench tests is the availability of an anatomically faithful model of the spinal microanatomy with deformable, fluid filled spinal compartment in which pulsatile CSF flow fields can be induced over a physiologically range.

In this paper, we will present parametric studies of IT infusion experiments in a subject-specific anatomically accurate 3D printed transparent replica of the human spinal subarachnoid spaces (SAS) with natural CSF pulsations within the physiological range of spinal fluid amplitude and frequency [11]. High-speed video recording enabled accurate observation of spatiotemporal dispersion patterns of tracers during high-volume IT injection and subsequently in the post infusion phase due to natural CSF oscillations. The results characterize dispersion speed of tracers as a function of infusion settings (infusion volume, flow rate, position, duration, catheter diameters) and natural physiological properties (=CSF stroke volume amplitude and frequency). We further compare the experimental data with prior theories developed for solute dispersion in oscillatory pipe flow.

Materials and Methods

In vitro Human Spine and Central Nervous System Model

We designed a deformable model of the human central nervous system (CNS) to reproduce functional biomechanical relations between dynamically interacting CSF compartments (Figs. 1a, b). Anatomically accurate analog of the spinal subarachnoid spaces (SAS) with transparent spinal

bioRxiv preprint doi: https://doi.org/10.1101/2022.03.22.485353; this version posted March 25, 2022. The copyright holder for this preprint (which was not certified by peer review) is the author/funder. All rights reserved. No reuse allowed without permission.

cord including pairs of peripheral nerve roots and the translucent dural surfaces were manufactured in a multistep 3D printing and casting procedure with subject-specific imaging data of a 26-year old male volunteer [11]. Spinal CSF motion was generated by transmitting oscillatory expansion and contraction of an inflatable balloon located in the head section to the fluid. The ballon, mimicking the cerebrocranial vascular bed, in turn was driven by a piston pump capable of generating stroke volumes up to 1ml/beat in the frequency range of 0-169 beats per minute. The mode of pulsatile flow conditions in the spinal fluid filled CSF-filled spaces of the bench model reproduces pulsatile vascular bed dilation consistent with our understanding of periodic intracranial CSF displacement [12]. More manufacturing details of the subject-specific CNS replica can be found elsewhere [13]–[15].

To reproduce conditions of in vivo IT procedures on the bench, infusion catheters were inserted into the lumbar and thoracic regions with inner diameters of 0.2 mm, 1.0 mm, and 3.2 mm. The elastic dura of the spine model has self-sealing property thus enabling realistic catheter insertion and placement similar to human clinical practice. A wide range of infusion parameters settings (=infusion volume, flow rate, position, duration) and systemic blood pump settings (=stoke volume and frequency) were able to implement a realistic spectrum of infusion scenarios (bolus, chronic drug pump) occurring in the physiological range of CSF oscillations and are listed in Appendix A. A total of 77 IT infusion experiments (E1-E77) of trypan blue (Sigma, Aldrich) released with a programmable syringe pump (Harvard Instruments) were performed to precisely investigate the correlation between dye dispersion, CSF pulsations and infusion parameters (Appendixes B and C).

bioRxiv preprint doi: https://doi.org/10.1101/2022.03.22.485353; this version posted March 25, 2022. The copyright holder for this preprint (which was not certified by peer review) is the author/funder. All rights reserved. No reuse allowed without permission.

Tracer dispersion tracking with videography

Automatic image processing. Snapshots were obtained from the experimental videos showing the dispersion of the tracer at different times. MATLAB 2019b was used for semi-automated image analysis and quantification of dye dispersion (Appendix D). A file system was designed to store the parameters of each experimental run: infusion volume, infusion molarity, infusion volumetric flow rate (IVF), experiment duration, subject orientation (supine), oscillation frequency, and oscillation amplitude. Each video frame captured red-green-blue (RGB) data in the range of 0 to 255 for each pixel at a location x and time. Analysis was divided into two phases: Phase-1, (acute infusion, t=0-1 min) covered the time the infusion pump actively discharged dye into CNS replica. Phase-2 (post infusion, t>1 min) further tracked dynamic tracer spread under the influence of natural CSF pulsations (without further infusion).

Optical analysis of tracer concentration. A calibration procedure (see details in Appendix D) acquired RGB triplet values for a set of reference samples with known concentrations. Linear least square fitting was performed to create a correspondence map between RGB intensities and reference concentrations (Appendixes E). The inverse of the calibration curve was used to infer *dye concentration* $C(x,t)$, at a particular position, x, along the neuraxis from *intensities* (=RGB values were averaged over the projection of a radial cross section, i.e. vertical image y-direction).

Analysis of the dispersion front. A custom image analysis code was used to determine speed and spatial position of the visible dye front. A binary mask shown in Fig. 1c was coded to separate the dye-filled space from the dye-free void space for time frames in 1 min intervals (Appendix D). This process extracts the pixel information from select video frames at the region of interest (ROI) that covers only tracer filled areas. (Fig. 1c). The masking process ensures that only RGB values pertaining to tracer filled spaces are stored before further analysis. The final pixel information

bioRxiv preprint doi: https://doi.org/10.1101/2022.03.22.485353; this version posted March 25, 2022. The copyright holder for this preprint (which was not certified by peer review) is the author/funder. All rights reserved. No reuse allowed without permission.

(=RGB values) is used for quantifying *concentration* (Fig. 1c) using the above mentioned calibration procedure.

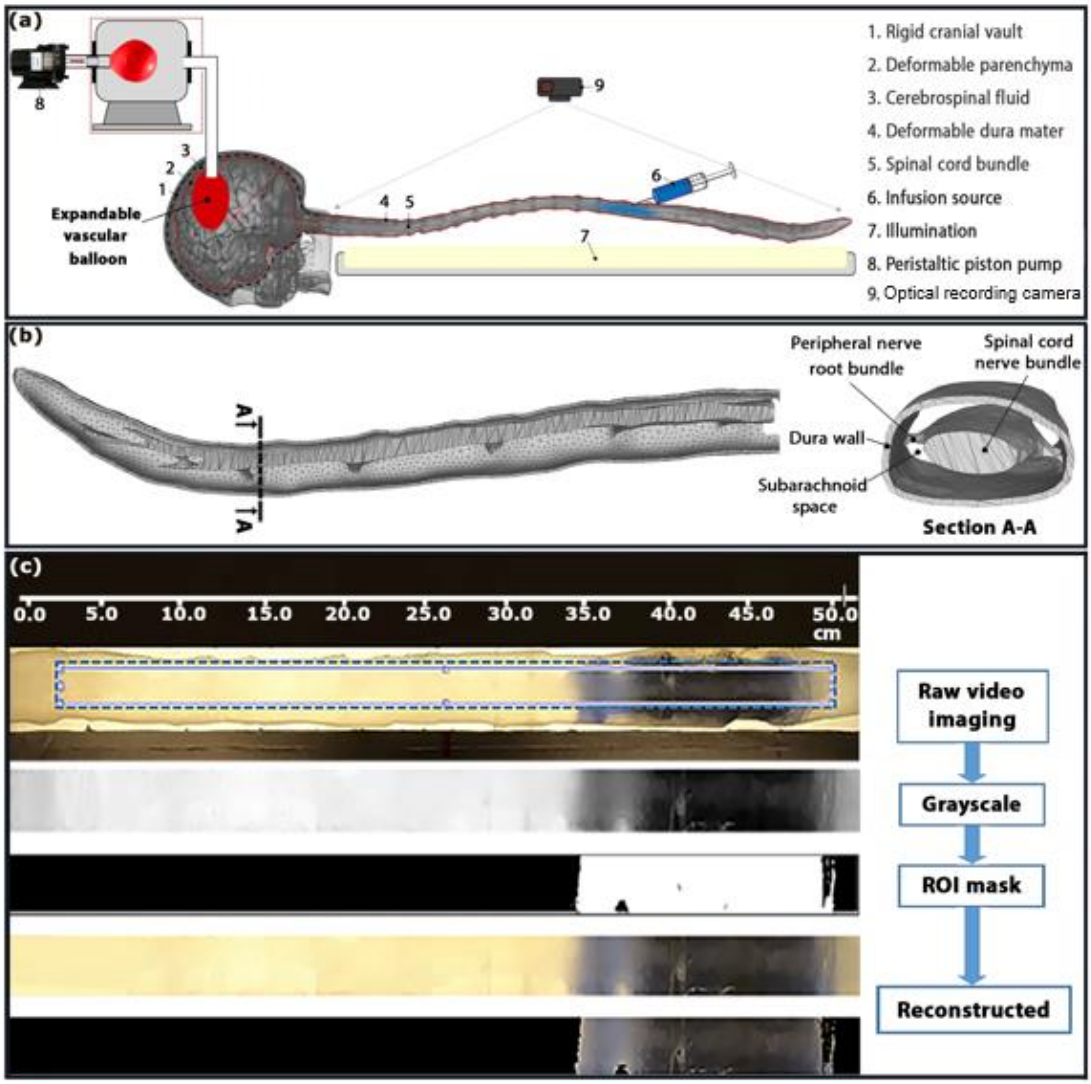

Fig. 1. Phantom geometry, and videography of the dispersion of infused tracer in the central nervous system flow surrogate model. (a) A schematic diagram of the experimental setting. (b) the meshed model of a subject-specific central nervous system spine phantom models with peripheral nerve roots obtained from MR images. (c) Depiction of workflow for image processing and analysis of the tracer infusions. The region of interest (ROI) is selected in the video frame. A greyscale image is created to develop an ROI mask for selecting where in the original frames the tracer exists. Pixels representing just the tracer in the frames of the video are selected with the ROI mask. ROI: region of interest.

bioRxiv preprint doi: https://doi.org/10.1101/2022.03.22.485353; this version posted March 25, 2022. The copyright holder for this preprint (which was not certified by peer review) is the author/funder. All rights reserved. No reuse allowed without permission.

Experimental determination of the speed of the advancement of the tracer front

The *method of moments* (MoM) was used to determine the apparent tracer dispersion velocity from video data, because it minimizes the sensitivity of optically acquired concentration profiles to uneven lighting conditions, scattering effects, and uncertainty in concentration inference from intensity data [16]. The MoM has been previously used to quantify dispersion in an annular tube [17]–[19]. We first determined the *speed of caudocranial motion* of the infusate by tracking shifts in the center of gravity of tracer profile. The first moment $m_1(t)$ of the observed concentration profiles at time t is calculated as in Eq. (1), where x is the position along the neuroaxis, x_0, marks the infusion point. The extreme limit of the ROI equal to full length from caudal to cranial aspects measured x_m=48 cm. In each time frame, t, the first moment, $m_1(t)$, gives the location of the center of gravity, $\bar{x}(t)$, of the tracer concentration profile at a time point, $C(x,t)$. The *speed of caudocranial motion* is equal to the change of the first moment with time.

$$m_1(t) = \frac{\int_{x_o}^{x_m} C(x,t)\, x\, dx}{\int_{x_o}^{x_m} C(x,t)\, dx} = \bar{x}(t) \tag{1}$$

We further computed the second moment or *area moment of inertia* for each time point as in Eq. (2). The second moment can be interpreted as the mean spread of the visible concentration profile around its center, $\bar{x}(t)$. The increase in its variance with time, $\sigma(t)^2$, is directly proportional to the apparent dispersion or diffusion rate D_{Ex1} of the tracer molecule as in Eq. (3). The coefficient of the apparent dispersion can then conveniently be determined as the rate of change in the second moment of the concentration curves by plotting their variance as a function of time.

$$m_2(t) = \frac{\int_{x_o}^{x_m} [x(t) - \bar{x}(t)]^2\, C(x,t)\, dx}{\int_{x_o}^{x_m} C(x,t)\, dx} = \sigma(t)^2 \tag{2}$$

bioRxiv preprint doi: https://doi.org/10.1101/2022.03.22.485353; this version posted March 25, 2022. The copyright holder for this preprint (which was not certified by peer review) is the author/funder. All rights reserved. No reuse allowed without permission.

$$D_{Ex1} = \frac{1}{2}\frac{\Delta\sigma(t)^2}{\Delta t} \quad (3)$$

Stroke volumes and mean pulsatile flow velocities for formal analysis.

In MR imaging, it is convenient to characterize natural CSF pulsations via the instantaneous total CSF volume, V(t), cervical stroke volume, v_c, and CSF angular pulse frequency, ω. We estimated the resulting average CSF flow velocity, U_{rms}, with Eq. (4) to translate data obtained from MR quantities to quantities in formal flow analysis (e.g TAD). Thus, two stroke volume settings of 0.5 to 1ml/beat in the frequency range of 0 to 120 beat/min enabled us to induce a wide range of CSF flow velocity averages covering the entire physiological range (0.09 cm/s – 0.93 cm/s).

The mean CSF flow velocity, U_{rms}, in the cervical region was computed by integrating and averaging the squared ratio of pulsatile volumetric flow rate, $\frac{dV(t)}{dt}$, divided by the hydraulic cross sectional area of the spinal CSF subarachnoid space, A, under cosine profile assumption as in Eq. (4), where V_0 is the initial volume of CSF in cm^3 in the system, N_{bpm} is the frequency in beat per minute, with period T in minutes.

$$U_{rms} = \sqrt{\frac{\int_0^t (V(t)/A)^2}{T}dt} \quad (4)$$

$$V(t) = V_0 + \left(\frac{v_c}{2}\right) - \left(\frac{v_c}{2}\right)\cos(\omega\, t), \quad A = \frac{V}{L}, \quad \omega = 2\pi\, N_{bpm}$$

Statistical analysis

Initially, each experiment was repeated six times with the same settings to ensure reproducibility and robustness of data acquisition. The results of the Shapiro-Wilk test indicated that all datasets had a normal distribution. ANOVA test was used in the regression analyses using IBM SPSS v26 to confirm that regression models described the dependent variables. Confidence intervals are calculated for all regression results. The Durbin-Watson statistic for all regression results was 2.075, therefore the datasets did not have autocorrelation. Furthermore, calculated

bioRxiv preprint doi: https://doi.org/10.1101/2022.03.22.485353; this version posted March 25, 2022. The copyright holder for this preprint (which was not certified by peer review) is the author/funder. All rights reserved. No reuse allowed without permission.

tolerances did not indicate the multicollinearity effect in any datasets. TA P-value of 0.05 was considered statistically significant.

Results

Dynamic tracer profile front tracking

Figure 2a depicts tracer concentrations profiles inferred from calibrated RGB pixel intensity as described in the methods section. Figs. 2b, c depict a time-lapsed series of images showing the expansion of the blue tracer before and after the infusion at time points 0s, 70s, 140s 210s, 280s, and 350s. The binary mask was used to crop images to the width of the spinal section covered by detectable tracer intensity. The size of this mask along the neuraxis (x-direction) is referred to as the *dispersion width* of the tracer at time t, DD(t). The next section shows systematic analysis of infusion and physiological parameters on the speed of tracer dispersion.

bioRxiv preprint doi: https://doi.org/10.1101/2022.03.22.485353; this version posted March 25, 2022. The copyright holder for this preprint (which was not certified by peer review) is the author/funder. All rights reserved. No reuse allowed without permission.

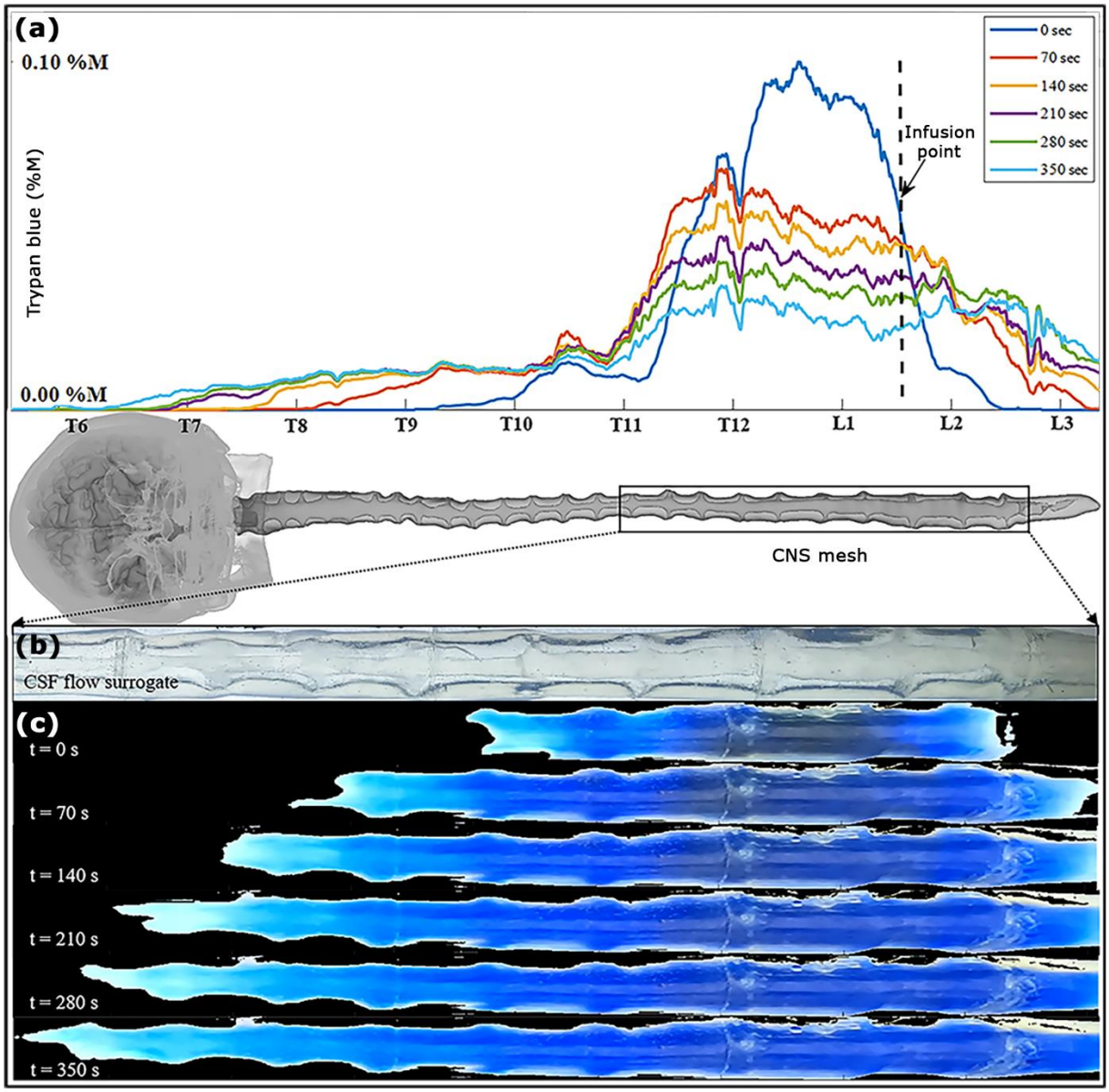

Fig. 2. Experimental dynamic tracking of the advancing trypan blue front. Data extracted from video recordings of infused tracer biodispersion experiments is processed and reconstructed into profile curves. (a) Overview of experiments and the time-lapsed images from a typical infusion experiment with IVF 2.0 ml/min, pulsation 1.0 ml/beat, and 0.1 %M of trypan blue concentration. It also shows a ruler with labels for the anatomical regions (i.e., cervical, thoracic, and lumbar) as well as the axial coordinate system, along the neuroaxis. (b) Depiction of optically clear cerebrospinal flow surrogate model before the injection (no blue dye is visible yet). (c) Progressing tracer front spreading from the injection site preferably in cranial direction. CSF: cerebrospinal fluid. IVF: infusion volumetric flowrate. CNS: the central nervous system.

bioRxiv preprint doi: https://doi.org/10.1101/2022.03.22.485353; this version posted March 25, 2022. The copyright holder for this preprint (which was not certified by peer review) is the author/funder. All rights reserved. No reuse allowed without permission.

Effect of catheter diameter on initial tracer spread (phase-1)

We studied the effect of catheter diameter on the speed and size of the dispersion front. Infusion experiments are performed using three different catheters with inner diameters of 0.2 mm (needle N1), 1.0 mm (N2), and 3.2 mm for widest needle (N3). Infusion lasted one minute over the course of 54 experiments (E1-E54 in Appendix B). Dispersion width after 10 min, DD (10 min) was measured from the point of the needle tip to the tip of the dye front in the caudal and cranial direction. The duration of 10 min was chosen, because this initial time window is critically important for assessing acute risks associated with high volume IT injection. High local toxicity has been implicated with granuloma formation [20], [21]. We also varied infusion volumetric flow rates (IVF= 0.5, 1.0, and 2.0 mL/min).

Fig. 3a shows that high caliber catheters promote slower tracer spread with shorter dispersion width, DD(1min). For identical infusion flow rate (IVFs from 0.5, 1.0, and 2.0mL/min), the large caliber needle (N3) had the shortest dispersion width. Fig. 3b depicts the effect of inner catheter diameter on the extent of the tracer spread observed 10 min after the infusion as a function of infusion flow. All experimental results (N=54) were also fitted into a linear regression model that can be used to estimate initial neuraxial coverage (=extent of the dispersion) as a function of catheter lumen and infusion volumes (IVF). The regression model of Eq. (5) can serve as a guideline in the clinical practice to estimate the length of initial dispersion as a function of catheter lumen and IVF (Fig. 3b).

$$\boldsymbol{DD}\ (10\ min) = a\ \ (\boldsymbol{ND}) + b\ \ (\boldsymbol{IVF})\ +\ \mathrm{c} \qquad (5)$$

where ND is the inner needle diameter. The $a, b, and\ c$ are -1.4133, 2.8428, and 19.92.

The realization of a fixed infusion rate with thinner catheters requires higher infusion pressure resulting in higher exit velocities (V_{Ext}) at their tips. Thus, catheter N1 at IVF= 2.0 ml/min has the

bioRxiv preprint doi: https://doi.org/10.1101/2022.03.22.485353; this version posted March 25, 2022. The copyright holder for this preprint (which was not certified by peer review) is the author/funder. All rights reserved. No reuse allowed without permission.

largest V_{Ext} and kinetic energy (KE) (Table 1). Also, exit velocity and kinetic energy of catheter N1 are higher than that of needles 2 and 3 with the same IVF. In thin catheters, a higher infusion impulse is delivered during the injection phase which translates in wider dispersion length in the observed tracer front for the same injection flow rate.

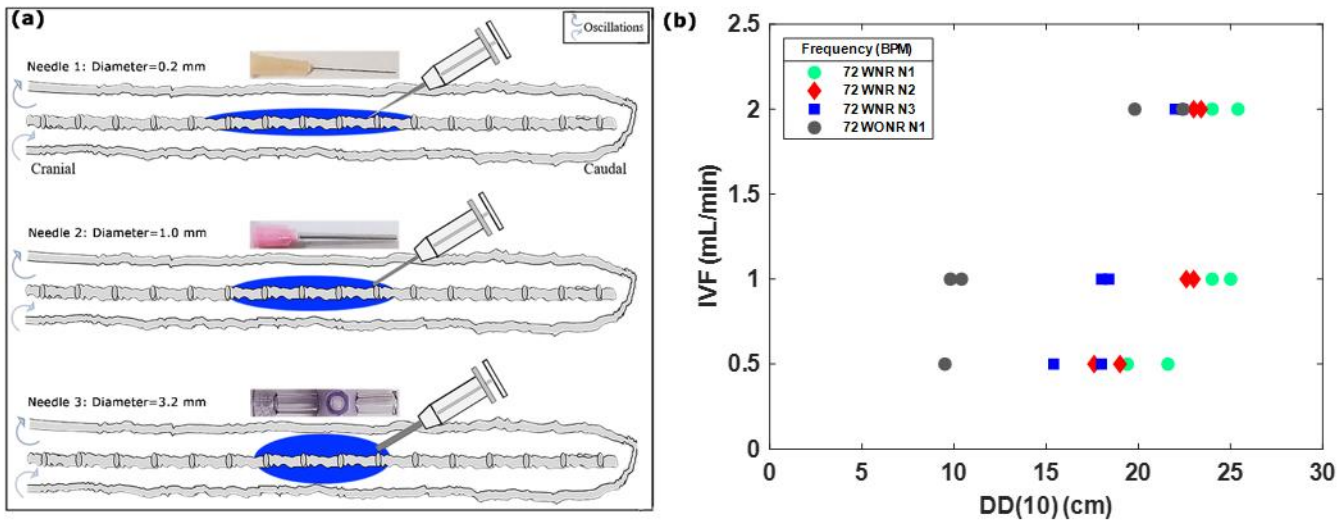

Fig. 3. Effects of needle diameter, IVF, and DD on tracer biodispersion. (a) The central nervous system (CNS) spine model is depicted as a diagram with varied diameter infusion catheters and corresponding idealized dispersion patterns (blue). (b) shows the relation of the infusion type to DD(10) and needle diameter in a CNS spine model with peripheral nerve roots (colorful) and without peripheral nerve roots (gray). DD(10) represents the linear dispersion distance the tracer front after 10 minutes of infusion. N1, N2, and N3 represent needles 1, 2, and 3, respectively. IVF: infusion volumetric flow rate. WNR: with nerve root. WONR: without nerve root.

Table 1. The exit velocities (V_{Ext}) and kinetic energies (KE) for needle 1, needle 2, and needle 3 repeated for three different infusion volumetric flow rate (IVF).

Needle type	IVF ($mL.min^{-1}$)	V_{Ext} ($m.s^{-1}$)	KE ($Kg.m^2.s^{-2}$)
Needle 1 (d= 0.2 mm)	0.5	0.2700	3.645e-2
	1.0	0.5300	1.405e-1
	2.0	1.0600	5.618e-1
Needle 2 (d= 1 mm)	0.5	0.0100	1.000e-4
	1.0	0.0200	2.000e-4
	2.0	0.0400	8.000e-4
Needle 3 (d= 3.2 mm)	0.5	0.0006	1.800e-7
	1.0	0.0011	6.000e-7
	2.0	0.0022	2.420e-6

bioRxiv preprint doi: https://doi.org/10.1101/2022.03.22.485353; this version posted March 25, 2022. The copyright holder for this preprint (which was not certified by peer review) is the author/funder. All rights reserved. No reuse allowed without permission.

Effect of injection parameters on initial caudocranial dispersion (phase-1, acute infusion)

Experimental settings of injection flow rate, injection volume, and catheter specifications were varied to explore optimal conditions for targeting the cervical section or brain area. Fifty-four experiments (N=54) were conducted to systematically characterize tracer targeting towards the cranial compartment as a function of infusion parameters (phase-1, depicted in Fig. 4A). The results in Fig. 4b show that higher infusion flow rates IVF accelerate the speed of the tracer front advancing in the cranial direction from the infusion catheter tip. The distance the tracer front moves in the cranial direction from the infusion catheter tip for the CNS model in the supine position as observed 10 mins after infusion is represented by $S_{DD.}$ This effect at high volume injections is due to the increased insertion kinetic energy (Table 1).

The speed of caudocranial motion, CCV, is calculated as the change of the first moment with respect to time as shown in appendix F. All experiments showed a shift of the first moment towards the cranium. We determined the speed of apparent caudocranial advancement of the tracer front, $\boldsymbol{CCV}$, by recoding its positions for different time points. The results of Fig. 4C show that the caudocranial advancement of the tracer front from the injection site towards the cranium slightly increased with oscillation frequency, $\boldsymbol{f}$, as indicated the regression of Eq. (6a) and $\boldsymbol{U_{rms}}$, as root-mean square velocity, as indicated the regression of Eq. (6b) with constant terms a and b as 0.3292 and 0.0023 for Eq. (6a), and 0.3420 and 0.0080 for Eq. (6b) respectively. At 1/ml stroke volume, this trend was similar but with a wider variability between runs (Fig. 4D)

$$\boldsymbol{CCV_f}\ (cm/min) = a\ \boldsymbol{f} + b \tag{6a}$$

$$\boldsymbol{CCV_{U_{rms}}}\ (cm/min) = a\ \boldsymbol{U_{rms}} + b \tag{6b}$$

bioRxiv preprint doi: https://doi.org/10.1101/2022.03.22.485353; this version posted March 25, 2022. The copyright holder for this preprint (which was not certified by peer review) is the author/funder. All rights reserved. No reuse allowed without permission.

The rapid expansion of the drug front follows qualitatively the amount of infused tracer as expected, because the main driver of initial tracer spread is the injection impulse of fresh infusate concentrated in the relative narrow spatial confinement in the lumbar injection zone.

Eq (7) obtained by regression analysis describes the dependence of the effective diffusion coefficient on CSF pulse frequency for the phase-1 (Figs. 4E , F). The terms a and b are constants which are obtained as 1.12 and 232.87 for stroke volume of 0.5mL/stroke and 3.62 and 232.63 for stroke volume of 1.0mL/stroke.

$$\boldsymbol{D_{Ex2}}(\mathrm{cm^2/min}) = a\ \boldsymbol{f} + b \qquad (7)$$

bioRxiv preprint doi: https://doi.org/10.1101/2022.03.22.485353; this version posted March 25, 2022. The copyright holder for this preprint (which was not certified by peer review) is the author/funder. All rights reserved. No reuse allowed without permission.

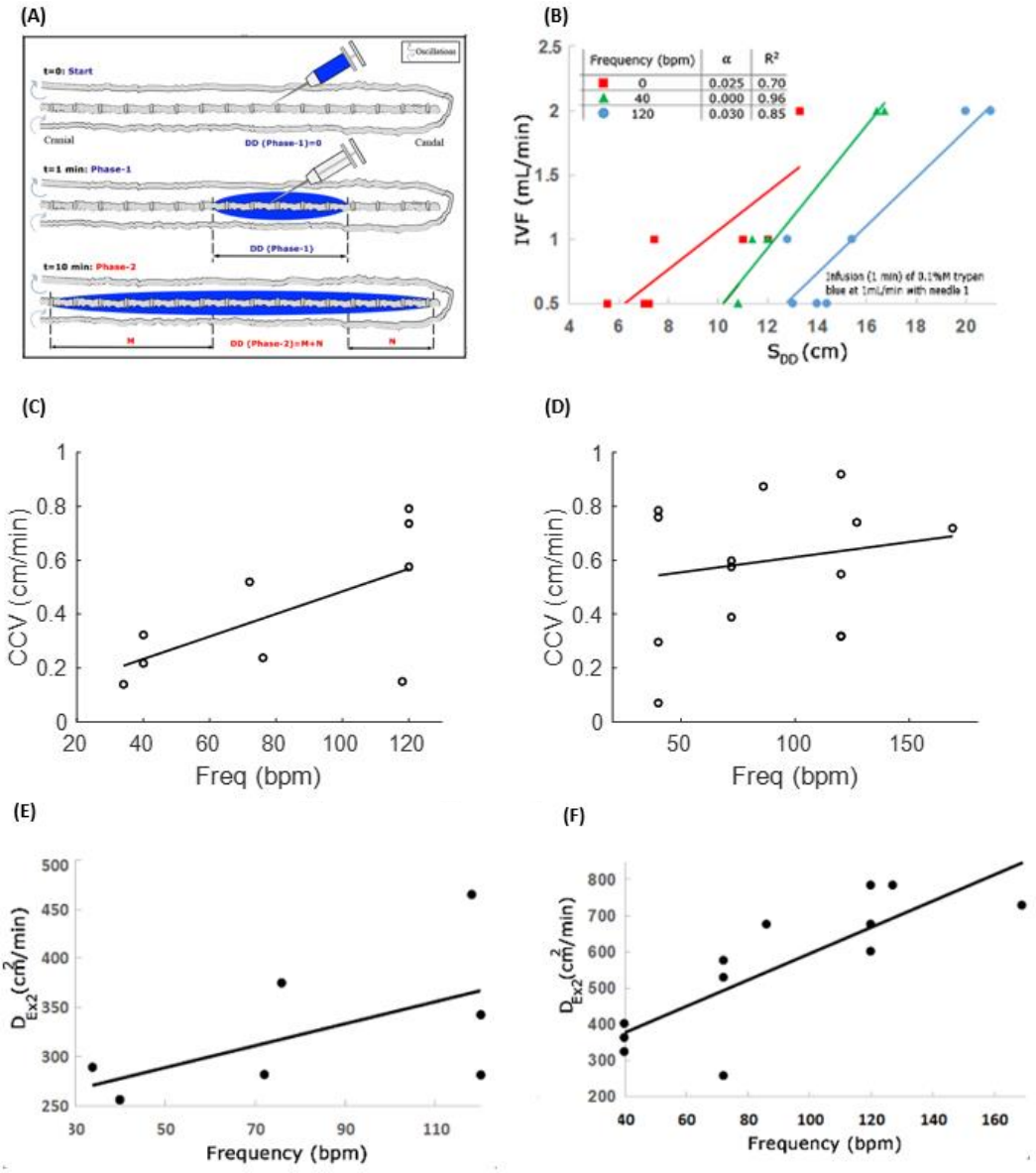

Fig. 4. (A) Schematic depicting experimental setting in phase-1 tracer dispersion experiments. All results pertain to injection phase (phase-1) (B) Effect of CSF oscillation frequency on dispersion length S_{DD} (with nerves) using IVF of 0.5, 1.0, and 2.0 ml/min under oscillation frequencies 0, 40, and 140 bpm. (C, D) The caudocranial velocity (CCV) changes of the tracer relative to frequency for pulsation for 0.5 mL/beat (C) and 1.0 mL/beat (D) respectively. At high infusion rates, frequency has a weak effect of S_{DD}. (E) Experimental diffusion coefficient of the tracer particles for oscillation frequency (34, 40, 72, 76, 118, 120 bpm) for 0.5 mL/beat, and (F) Oscillation frequency (40, 72, 86, 120, 127, 169 bpm) for 1.0 mL/beat. Experiment parameters are as follows: IVF (1.0 mL/min), infusion volume (1.0 mL), tracer (0.1% trypan blue), and orientation (supine). DD represents the linear dispersion distance the tracer front moves in the caudal and cranial direction from the infusion catheter tip. S_{DD} represents the linear dispersion distance the tracer front moves in the caudal and cranial direction from the infusion catheter tip while the CNS model is in the supine position. D_{Ex2} represents the calculated dispersion coefficient. IVF: infusion volumetric flow rate.

bioRxiv preprint doi: https://doi.org/10.1101/2022.03.22.485353; this version posted March 25, 2022. The copyright holder for this preprint (which was not certified by peer review) is the author/funder. All rights reserved. No reuse allowed without permission.

Dispersion by natural CSF pulsation (phase-2, post injection)

Once the infusion stops (t >1min), further tracer spread is no longer propelled by injection impulse. It has long been known in the engineering community that oscillatory flow enhances solute dispersion, a phenomenon often referred to as Taylor-Aris dispersion (TAD). CSF flow spinal subarachnoid space is also oscillatory with zero net flux in our model. This is also approximately valid in vivo since bulk CSF production rates are much smaller than oscillatory fluxes.

The apparent dispersion coefficient of tracer spread in oscillatory CSF flow was determined experimentally (N=24) as a function of amplitudes (cervical CSF stroke volume, mean CSF flow velocities) and frequencies in a series of dynamic tracer infusion experiments. Two stroke volume settings of 0.5 to 1ml/beat in the frequency range of 0 to 120 beat/min enabled us to induce a wide range of CSF flow velocity averages covering the entire physiological range (0.09–0.93 cm/s). Tracer dispersion was rapid reaching the cervical region in less than ten minutes, and it spread quickly throughout the spinal subarachnoid space (SAS). Experimentally obtained (=method of moments, MoM) dispersion coefficients, D_{ex1}, summarized in Fig. 5 confirm our earlier finding [22], [23] that CSF amplitude and frequency are the critical factors of IT drug dispersion with D_{Ex1}=2.0–3.95 cm^2/min for a 0.5 mL/beat stroke volume, and D_{Ex1}=4.41-11.69 cm^2/min for the 1 mL/beat stroke volume.

The correlation between apparent diffusion coefficient and CSF pulsations in Eq. (8), a function of CSF stroke volume was established using the table G2 and table G3 in appendix G. It allows clinicians to estimate the effective dispersion in an intrathecal experiment as a function of the stroke volume in the cervical region, as well as the frequency of the CSF pulsations.

We also created a correlation between apparent diffusion coefficient and CSF pulsations in Eq. (9a), a function of root-mean-square velocity of Eq. (9b). The mean CSF flow velocity, U_{rms}, in the cervical region was computed as described in the methods section.

$$D_{dim} = a + b\, v_c + c\, f \tag{8a}$$

$$D_{dim} = A + B\, U_{rms} + C\, f \tag{8b}$$

Where a, b and c are constant which are given as 1.6056, 4.3573, and -0.7001 for 0.5mL/Stroke, and 3.6672, -0.4698, and 0.0328 respectively for 1mL/Stroke. Also, where A, B and C are constant which are given as 1.2566e04, 0.0252, and -2.7918e-4 for 0.5mL/Stroke, and 6.4646e3, -0.0038, and 8.9389e-5 respectively for 1mL/Stroke. v_c is the stroke volume, U_{rms} is the root-mean-square

bioRxiv preprint doi: https://doi.org/10.1101/2022.03.22.485353; this version posted March 25, 2022. The copyright holder for this preprint (which was not certified by peer review) is the author/funder. All rights reserved. No reuse allowed without permission.

velocity of the CSF, f is the frequency and D_{dim} is the experimental dispersion coefficient for the dimensional model. This dimensional formula and the relationship supported by the data is given in Fig. 6A.

bioRxiv preprint doi: https://doi.org/10.1101/2022.03.22.485353; this version posted March 25, 2022. The copyright holder for this preprint (which was not certified by peer review) is the author/funder. All rights reserved. No reuse allowed without permission.

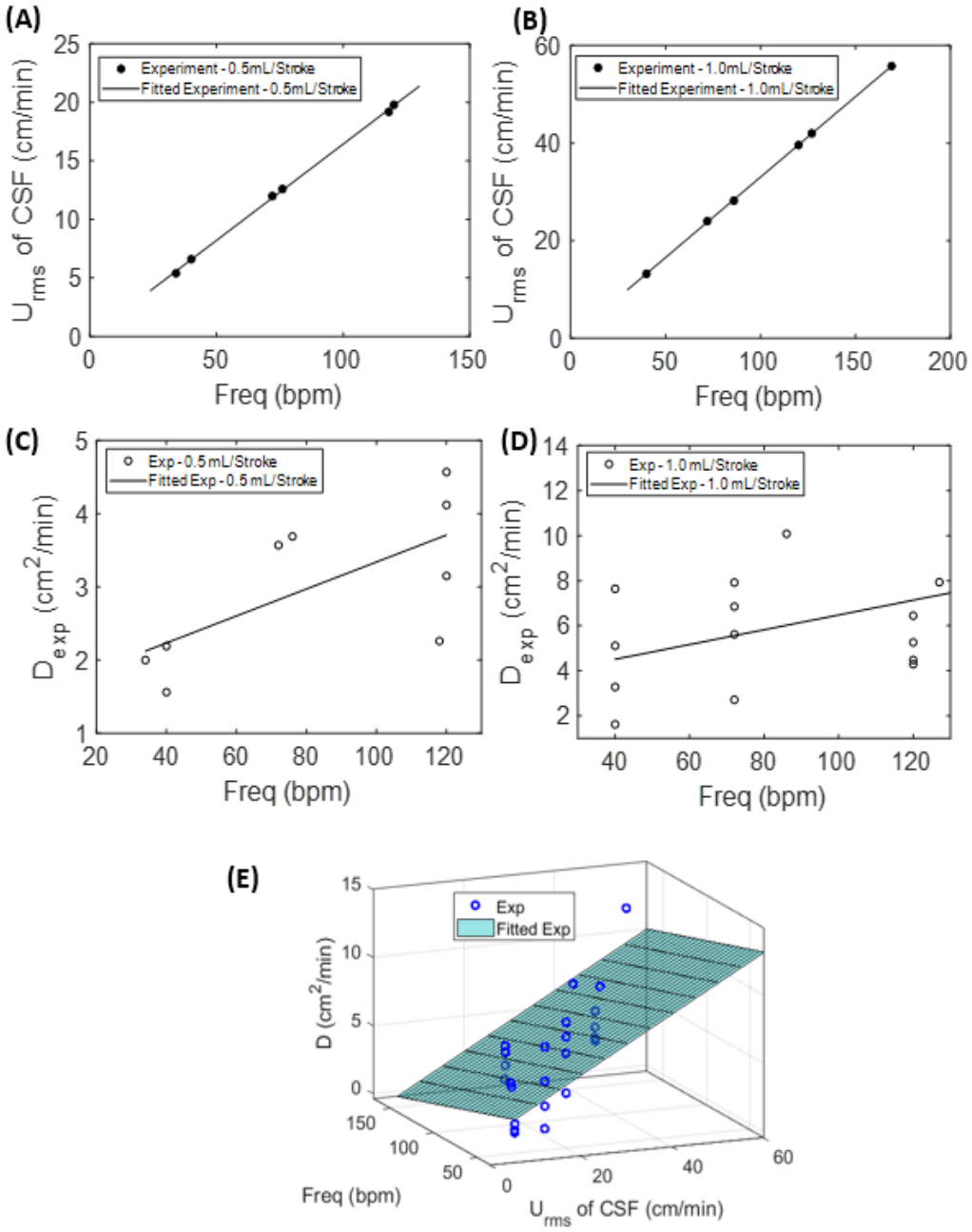

Fig. 5 . The root-mean-square velocity of the CSF at different frequencies for 0.5 mL/beat (A) and 1.0 mL/beat (B) respectively. Experimental diffusivity of infusion at different frequencies for 0.5 mL/beat (C) and 1.0 mL/beat (D). Relation of root-mean-square velocity of the CSF, frequency, and experimental diffusivity (E). In these results, 2 mL of 0.4 %M trypan blue was infused for 1.0 minutes as the infusion parameter. D represents the calculated dispersion coefficient.

bioRxiv preprint doi: https://doi.org/10.1101/2022.03.22.485353; this version posted March 25, 2022. The copyright holder for this preprint (which was not certified by peer review) is the author/funder. All rights reserved. No reuse allowed without permission.

Effect of nerve roots on dispersion distance in phase-2

We observed previously that annular phantoms without microanatomical features have slower dispersion [24], [25]. To test the significance of microanatomical features on tracer dispersion, we also fabricated a spinal model without nerve roots and compared tracer dispersion during infusion to the more anatomically realistic model with nerve roots. Tracer dispersion in the model with nerve roots is always much more rapid than in a system lacking nerve roots under the same condition of oscillatory flow (Fig. 3b and Appendix B). Complex flow and mixing patterns observable are absent in idealized annular models lacking spinal microanatomy [3], [26], [27], thus failing to boost the effective dispersion of IT injected tracers as this is the case when microanatomical features are present (see Appendix B). The results of this study provide further evidence for the significant impact of microanatomical features on the spatial and temporal dispersion patterns of IT administered solutes shown previously [11].

Is IT drug biodistribtion predicted by Taylor-Aris Dispersion (TAD) theory? Several authors [13], [27], [28] tried Taylor-Aris dispersion theory and its extension by Watson [29] to predict the intrathecal drug dispersion. Here we tested whether the Taylor-Aris-Watson (TAW) approach matches tracer dispersion in the bench infusion tests. Watson's studies on solute dispersion in oscillatory pipe flow [29] based on prior work by Taylor [30] lead to analytical series solutions for the dispersion coefficient, D_{3D}, in rectangular channels as a function of average velocity and frequency of the oscillatory flow field. Based on this work, Lee [4] reports the asymptotic limit of the dispersion coefficient D_{3D} of the solute in terms of group Schmidt, Sc, Peclet number, Pe, and dimensionless frequency, Ω, as in Eq. (9), where U_{rms} are the mean velocity, ω its oscillation frequency, ν the kinematic viscosity of the bulk fluid. The channel cross sectional dimensions are height and width h and w.

bioRxiv preprint doi: https://doi.org/10.1101/2022.03.22.485353; this version posted March 25, 2022. The copyright holder for this preprint (which was not certified by peer review) is the author/funder. All rights reserved. No reuse allowed without permission.

$$\frac{\mathrm{D}_{3D}\Omega^2}{Pe^2} = \frac{Sc^{-1/2}}{\sqrt{2}(1+Sc^{-1})(1+Sc^{-1/2})}(1+\chi)\sqrt{\Omega} \tag{9}$$

with $$Sc = \frac{\nu}{D}\ Pe = \frac{U_{rms}\,h}{D}, \Omega = \frac{\omega\,h^2}{D}\ , \chi = \frac{h}{w}$$

Actual dispersion coefficients and those predicted by the TAW as a function of the Peclet number and dimensionless frequency are shown in Fig. 6B. The mean CSF flow velocity, U_{rms}, in the cervical region was computed as described in Eq. (4). It should be noted that in the CNS, the CSF velocity is graded along the neuraxis as a result of the spinal compliance[14] with the largest value in the cervical region and almost as zero in the sacral. In our analysis, we used the cervical U_{rms} for computing the Peclet number, so that the dispersion predicted by the TAD would be overestimated.

bioRxiv preprint doi: https://doi.org/10.1101/2022.03.22.485353; this version posted March 25, 2022. The copyright holder for this preprint (which was not certified by peer review) is the author/funder. All rights reserved. No reuse allowed without permission.

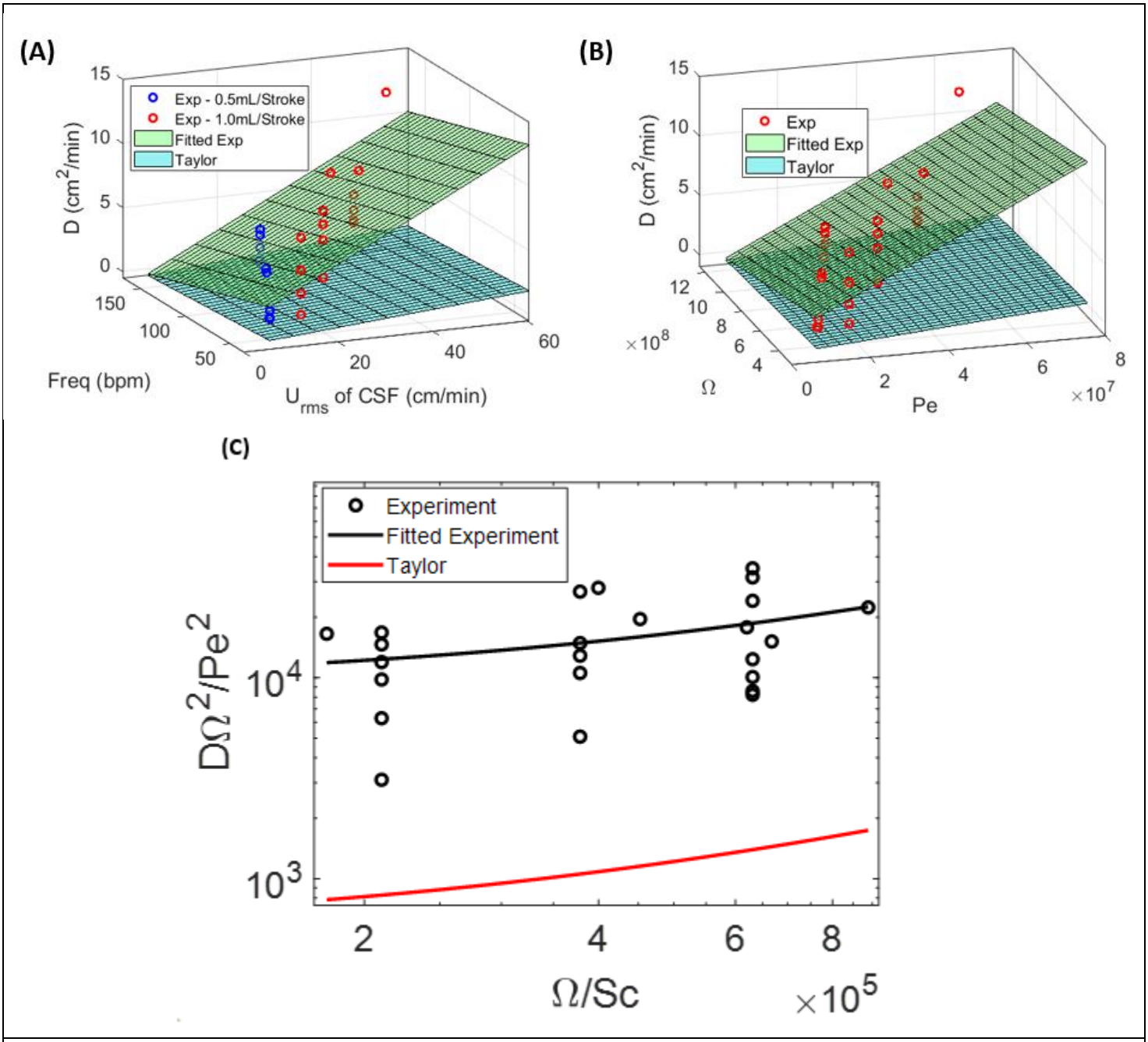

Figure 6. (A) The dispersion coefficients versus frequency at different root-mean-square velocity. The red and blue circles are experimental obtained dispersion coefficients at different frequencies and stroke volumes. (B) The dispersion coefficient as a function of the dimensionless numbers, Peclet number and dimensionless frequency (C)The dimensionless pairing of the dispersion coefficient with Peclet number and dimensionless frequency.

1

2 The data suggest that dispersion in IT experiments is much faster than predicted by TAD theory

3 over the entire physiological range. Fig.7a shows the relationship between the experimental and

bioRxiv preprint doi: https://doi.org/10.1101/2022.03.22.485353; this version posted March 25, 2022. The copyright holder for this preprint (which was not certified by peer review) is the author/funder. All rights reserved. No reuse allowed without permission.

theoretical dispersion coefficients for stroke volume of 0.5 and 1.0mL/ beat. Fig. 7b shows the comparison of the dispersion coefficient obtained experimentally and using Taylor analysis for all the studied stroke volumes and frequencies. Also, the pioneering Monte Carlo simulation work by Stockman [31] on dispersion analysis in spinal subarachnoid space was also plotted. While the trends are correctly given, Stockman's simulations predict about two times slower dispersion speeds that observed in our in vitro model. Fig. 7 also shows that the average dispersion coefficient obtained by the experiment is about 12 times bigger than that predicted by TAW.

bioRxiv preprint doi: https://doi.org/10.1101/2022.03.22.485353; this version posted March 25, 2022. The copyright holder for this preprint (which was not certified by peer review) is the author/funder. All rights reserved. No reuse allowed without permission.

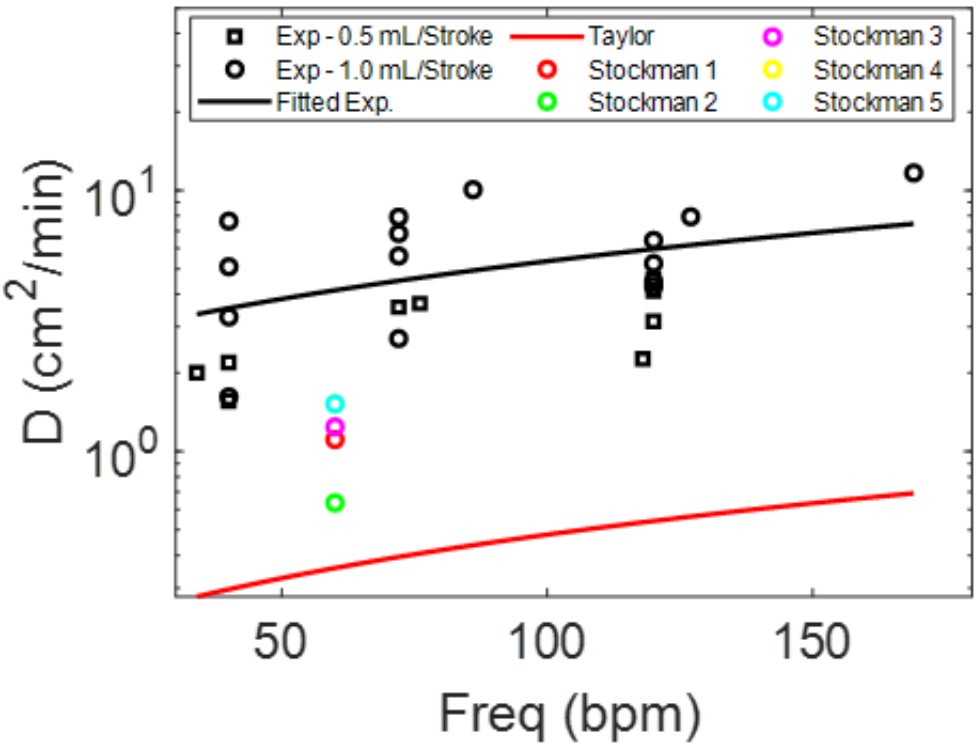

Fig. 7. The comparison of the dispersion coefficient obtained experimentally, and Taylor analysis for all stroke volumes. (i.e., 0.5 and 1.0 mL/Stroke) and different frequencies. The Stockman models were also used for frequency of 60bpm and stroke volume of 3.927e-6 mL/sec. Experimental values are from infusion experiment parameters of the following: 0.4% trypan blue infusion, IVF 2.0 mL/min, infusion volume 2.0 mL, supine orientation, with nerve roots, oscillation frequency of 34, 40, 72, 76, 118, and 120 bpm for 0.5 mL/beat and 40, 72, 86, 120, 127, and 169 bpm for 1.0 mL/beat. Where Stockman 1 – Stockman Spinal Model D, Stockman 2 – Stockman Model B-Normal, Stockman 3 – Stockman Model B-Dense, Stockman 4 – Stockman Model D-Normal, Stockman 5 – Stockman Model D-Dense.

bioRxiv preprint doi: https://doi.org/10.1101/2022.03.22.485353; this version posted March 25, 2022. The copyright holder for this preprint (which was not certified by peer review) is the author/funder. All rights reserved. No reuse allowed without permission.

Reduced order pharmacokinetic model for IT drug biodistribution

Experimental data for tracer infusion experiments served as input for a reduced order pharmacokinetic model of IT administration. The full description of this mechanistic drug administration model is beyond the scope of this manuscript but can be found elsewhere [32]. In brief, tracer biodispersion after lumbar intrathecal injection was simulated via a convection-diffusion process distributed along the neuraxis in Eq. (10). The effect of geometry induced mixing due to natural CSF pulsations was captured via the effective diffusivity, D_{eff}, determined in experiments described in methods and results sections. Sensitivity of predictions to infusion settings was incorporated via a single source term, V_{inj}(x,t). The effect of injection flow rate, volume and duration on the forces between infusate, spinal CSF interacting with deformable subarachnoid spaces (=dura) was accounted for by biomechanical fluid structure interaction (FSI). Accordingly, high volume injections generate a non-zero caudocranial convection term, U_{fsi}, during infusion (phase-1). After the infusion stops (phase-2), tracer continues to spread away from the lumbar injection site in accordance with effective dispersion as in Eq. (10).

Tracer concentration profiles along the neuraxis as a function of time were predicted with mechanistic pharmacokinetic simulations. Pharmacokinetic tracer profile simulations with CNS dimensions and infusion settings used in the experiments took less than one CPU minute to converge generating asymmetrical profiles with peak concentration decreases with time (Fig. 8a). The comparison with the experimental run shows a qualitatively match both the spatial and the temporal dimension as shown in Fig. 8a. Fig. 8b shows maximum concentration is attained in a short interval of mean path length. The preliminary results of the prosed order model shows that the use of experimentally obtained effective dispersion coefficients can effectively predict drug dispersion after IT administration using a reduced order pharmacokinetic simulations. It is worth

bioRxiv preprint doi: https://doi.org/10.1101/2022.03.22.485353; this version posted March 25, 2022. The copyright holder for this preprint (which was not certified by peer review) is the author/funder. All rights reserved. No reuse allowed without permission.

noting that simulation of biodistribution of active drugs into the CNS and the systemic circulation required additional information on biochemical parameters (denoted by the sink term $R(c,x)$) in Eq. (10) that might include drug half life, tissue uptake and clearance[14].

$$\frac{\partial C(x,t)}{\partial t} = \vec{\nabla}\left[D_{eff}\vec{\nabla}C(x,t)\right] - U_{fsi}(x,t,V_{\text{inj}})\,\vec{\nabla}C(x,t) + n_{\text{inj}}(x,t) - R(c,x) \quad (10)$$

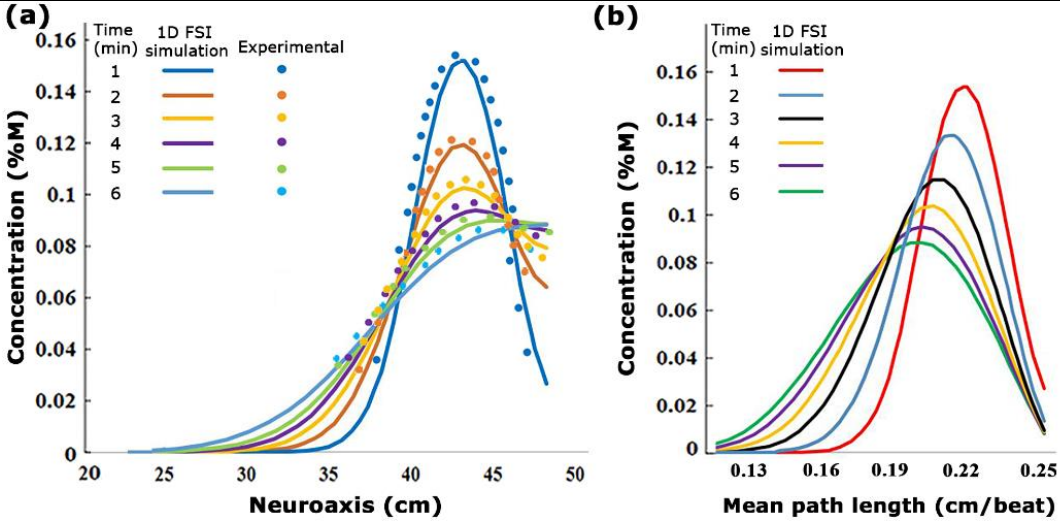

Fig. 8. (a) A visualization of the experimentally derived concentration values compared to the 1D fluid-structure interaction (FSI) simulation concentration values at different times. (b) changes of 1D FSI simulation concentration diagrams in the different mean path lengths. The values are from infusion experiment parameters in $0.5\ mL/beat$.

bioRxiv preprint doi: https://doi.org/10.1101/2022.03.22.485353; this version posted March 25, 2022. The copyright holder for this preprint (which was not certified by peer review) is the author/funder. All rights reserved. No reuse allowed without permission.

Discussion

Realistic replica of the human CNS. IT infusion studies under physiological conditions require deformability of the CSF spaces to accommodate realistic pulse pressure propagation and fluid motion inside a closed spinal SAS. Deformable fluid-filled spaces in the present bench test analog of the human CNS are fully enclosed between the soft dura/parenchyma surfaces and a distensible vascular interface (cranium vault with distensible vascular balloon) without leaving open system boundaries. The proposed configuration approximates the anatomy and fluid structure interaction dynamics of the spinal SAS, so we have confidence that it reproduces the complex geometry induced CSF mixing patterns that were reported in previous work using direct numerical simulation of spinal CSF flow [11]. The CNS model also incorporates microanatomical features of a spinal cord, epidural space and peripheral nerve root bundles, especially, which are critical geometric aspects implicated with enhanced mixing of fluid layers in the spinal SAS leading to accelerated drug dispersion.

Moreover, transparent borders of the see-through human CNS replica enabled dynamic optical tracking of tracer concentration profiles during and after IT solute administration. Our experiments characterized in detail two stages occurring during high volume IT infusion: The initial phase during which the drug is injected lasts only a few minutes in clinical settings. The duration of 10 min was chosen, because it is suitable for assessing acute risks associated with high volume IT administration (local toxicity, granuloma formation).

Injection phase. The axial dispersion during the injection phase (phase-1) correlated with infusion volume, IVF, and catheter diameters. Thinner catheters (inner diameter d=0.2 mm), generate wider and fast initial solute dispersion as is attainable with high caliber catheters (di=3.2 mm inner diameter). Based on our series of experiments, a simple formula in Eq (5) predicts initial

bioRxiv preprint doi: https://doi.org/10.1101/2022.03.22.485353; this version posted March 25, 2022. The copyright holder for this preprint (which was not certified by peer review) is the author/funder. All rights reserved. No reuse allowed without permission.

dispersion width, DD(10), the distribution length after 10 minutes of injection, as a function of injection volume/flow rate and catheter diameter. The formula in Eq. (5) may serve to estimate initial volume of distribution, peak concentrations and initial neuronal tissue exposure during the acute infusion phase of high-volume drug administration as a function of catheter lumen and infusion flow rate. Peak local toxicity risk may be elevated in infusion protocols generating narrower initial spread (i.e. high-volume infusion with large caliber catheters). It can also be used to estimate the expected local volume of drug action and local drug concentration to assess the risk of granuloma formations [21].

Under extremely low flow rate settings such as used in drug pumps, the effect of the injection impulse may be negligible. Accordingly, chronic administration with drug pumps may be governed by conditions of natural oscillation (phase-2) for its entire time course discussed below. For more recent developments for effective infusion protocols from drug pumps we refer to the work by Yaksh [33].

Dispersion in naturally oscillating CSF (after the injection subsides). After in the injection ceases, the tracer is further dispersed due to natural CSF pulsations. Oscillatory fluid flow around microanatomical features create geometry induced mixing pattern which break the laminar flow field by introducing eddies and vortices around nerve roots. Localized and interspersed eddies were observed in the flow directly upstream and downstream of cylindrical peripheral nerve root bundles suspended in the flow (see video in supplementary information). Moreover, trabeculae can substantially enhance this effect as reported in [11].

Caudocranial motion. In all infusion experiments, slow but steady caudocranial advancement of tracer front from the lumbar injection site towards the cranium was observed. We offer two explanations for experimentally observed caudocranial dye spread.

bioRxiv preprint doi: https://doi.org/10.1101/2022.03.22.485353; this version posted March 25, 2022. The copyright holder for this preprint (which was not certified by peer review) is the author/funder. All rights reserved. No reuse allowed without permission.

First, lumbar injection divides the space available for the solute to disperse into a smaller distal volume containing the sacral compartment and a larger cranially facing domain stretching from the catheter tip to the thoracic, the cervical and the cranial SAS. We observed that tracers initially spread equally in both sections which is consistent with a diffusive process. Subsequently, the advancing dye fronts fill the closed sacral domain faster due to its smaller size. Once the closed sacral region is filled, the tracer profile center of gravity begins shifting towards the head. The boundary effect causing asymmetric caudocranial tracer profiles was confirmed with a mechanistic diffusive transport model. Systematic experiments with varying CSF conditions (amplitude and frequency) enabled determination of a formula for the velocity the caudocranial shift as a function of CSF pulsations and frequency as in Eq (6).

The graded biomechanical deformation profile of the spinal SAS responsible for CSF pulse attenuation is a second factor. CSF pulse amplitude was shown to diminish gradually from the cervical towards the sacral region [34]. The CSF pulsations and average oscillatory CSF velocities, U_{rms}, become larger towards the cervical region compared to the lumbar region where the pulse amplitude is almost zero; thus, effective dispersion tends to become faster in caudocranial direction.

The infusion experiments were conducted in a closed CNS model with no net CSF generation or removal. This supports the notion that bulk CSF flow or absorption is *not necessary* for caudocranial drug dispersion to occur. Rather, experiments suggest that caudocranial transport of infused solutes can simply result from the asymmetry of the CSF spaces and graded CSF pulse amplitudes.

Recently, a very interesting analytical solution was developed by Lawrence et al. 2019 [13] to understand the dispersion of drugs in the SAS. Predictions of dispersion inside pulsatile flow inside

bioRxiv preprint doi: https://doi.org/10.1101/2022.03.22.485353; this version posted March 25, 2022. The copyright holder for this preprint (which was not certified by peer review) is the author/funder. All rights reserved. No reuse allowed without permission.

an idealized annulare geometry without the presence of microantomical features (e.g., nerve roots). also found solute transport controlled by convection with negligible Taylor dispersion. Numerical simulation experiments within the cervical subarachnoid space [35] also showed that the presence of spinal cord nerve roots increases drug dispersion. This result provide supporting evidence for our prior theoretical studies and experimental results presented here.

Derivation of clinical guidelines from in vitro experiments. Tracer dispersion was rapid reaching the cervical region in less than ten minutes, and it spread quickly throughout the spinal subarachnoid space (SAS), much faster than predicted by the TAD model. The apparent dispersion coefficient was robustly determined experimentally as a function of CSF amplitudes and frequencies. An empirical correlation (Eq. 8) between apparent diffusion coefficient and CSF pulsations, a function of CSF amplitude and oscillation was established. This formula is of clinical interest to predict tracer dispersion for intrathecal drug administration.

We provide a simple guideline for estimating the volume of distribution of the drug during the injection phase as a function of catheter caliber and injection volume based on the experimental data and model in Eq. (5). Table 2 summarizes the expected size of the injection front (dispersion length after 10 min) from the lumbar injection site. It can also be used to get an idea about the advancement from the injection site towards the cranium, since the moving front of the tracer prfile advances at least half of DD(10).

Table 2. Guide for caudocranial motion, DD(10) as a function of injection needle diameter (top row) and infusion volumetric flow rate (first column).

caudocranial motion from injection site (cm)	0.1 mm^{++}	0.2 mm	0.5 mm	1.0 mm	1.5 mm	3.2 mm
0.25 mL/min^{+}	20.49	20.34	19.92	19.21	18.51	16.10
0.50 mL/min	21.20	20.06	20.63	19.92	19.22	16.82
1.00 mL/min	22.62	22.48	22.05	21.35	20.64	18.24
2.00 mL/min	25.46	25.32	24.90	24.19	23.48	21.08
2.50 mL/min	26.88	26.74	26.32	25.61	24.90	22.50

$^{+}$Infusion volumetric flowrate, $^{++}$Inner diameter

bioRxiv preprint doi: https://doi.org/10.1101/2022.03.22.485353; this version posted March 25, 2022. The copyright holder for this preprint (which was not certified by peer review) is the author/funder. All rights reserved. No reuse allowed without permission.

For tracer dispersion in oscillatory CSF flow (phase-2), eq (9a) quantifies effective dispersion as a function of stroke volume and pulse frequency. The Table 3 derived from these data enables estimation of the effective dispersion coefficient for clinical applications. For drug molecules with different molecular diffusion coefficients (i,e. drugs with substantially different properties of our tracer), it may be used as a first approximation when no data are available or when its *Pe* number is in the same range as for trypan blue with diffusion coefficient of $D=1.938e^{-4}$ cm^2/min.

Table 3: The table of clinical data, Dispersion Coefficient D

D (cm^2/min)		Stroke volume ml/bt**				
		0.25	0.5	0.7	1.0	1.5
frequency bpm*	40	0.38	1.83	3.00	4.74	7.65
	60	0.94	2.39	3.55	5.30	8.21
	80	1.49	2.95	4.11	5.86	8.77
	100	2.05	3.51	4.67	6.42	9.32
	120	2.61	4.06	5.23	6.97	9.88
	140	3.17	4.62	5.79	7.53	10.44

*bmp – frequency of the CSF pulsation in beats per minute

**ml/b – stroke volume of the CSG flow in the cervical region

Note that the Schmidt number did not vary in our IT experiments, because CSF viscosity and molecular diffusivity of the tracer are constant. This is not a major restriction because drug dispersion operates typically in the high Schmidt number limit (in Eq. 9). where the authors [4] maintain that it is a very weak factor. Moreover, viscosity of CSF is fixed in intrathecal drug delivery.

Comparison to Taylor-Aris dispersion theory.

The analytical Taylor-Aris-Watson approach was shown to underestimate the actual dispersion in vitro by about 12 times, despite our choice to use the maximum (=cervical) mean CSF velocity in the Peclet number. This is not entirely unexpected since several factors present in intrathecal drug dispersion do not meet the strong assumptions in TAW approach. First, TAW does not account for geometry induced mixing by micro-anatomical features. It also does not consider the

bioRxiv preprint doi: https://doi.org/10.1101/2022.03.22.485353; this version posted March 25, 2022. The copyright holder for this preprint (which was not certified by peer review) is the author/funder. All rights reserved. No reuse allowed without permission.

effect of injection volume, catheter geometry and placement as discussed during phase-1 of the infusion experiments. Moreover, CSF flow with complex micro mixing occurs in a deformable spinal subarachnoid space, while TAW concerns rigid boundaries. Finally, CSF flow amplitudes are graded along the neuraxis, whereas TAW assumes constant flow velocity throughout the channel.

Eccentricity and stagnation zones. Several authors have implicated eccentricity of idealized cross sectional areas of CSF filled spaces in the spinal subarachnoid space as a key factor for accelerated drug dispersion [28], [34], [36]. The insensitivity to centric or eccentric alignment in our experiments does not seem to support the notion of eccentricity as a significant factor for the speed of IT dispersion. Moreover, we could not observe stagnation or recirculation zones in any of the experiments.

Limitations. There are safety limits to high volume injections adding the CSF amount during drug administration. We have experienced in rat that no more than 10% of the CSF volume can be safely injected over a period of a couple of minutes [37]. Higher injection impulse may also contribute to the possibility of high shear rates that nerve roots experience near the catheter tip, which may again pose an additional risk that requires clinical investigation.

The biomechanical stress-strain relation of the epidural spaces is a function of several poorly understood factors. These include viscous resistance exerted by venous blood volume and fatty tissues, possible elastic deformation resistance of nerve roots bulging into peripheral distal spaces, and the biomechanical properties of the dura membrane including the stiffening effect of by trabeculae and ligaments. The current model was able to induce cervical CSF displacements (stroke volume 0-1 ml/beat) within the physiological range, but was not designed to faithfully

bioRxiv preprint doi: https://doi.org/10.1101/2022.03.22.485353; this version posted March 25, 2022. The copyright holder for this preprint (which was not certified by peer review) is the author/funder. All rights reserved. No reuse allowed without permission.

reproduce the biomechanical compliance of the spinal compartment. Accordingly, we also did not attempt to measure absolute pressure changes that occur during infusion. We plan to study the rise in the line pressure or the increase in pressure in CSF of the spinal SAS as a function of injection parameters in future work.

Another related limitation pertains to the practice of fluid removal before high volume injection (initial CSF tapping). There was no attempt made to interrogate the CNS model regarding biomechanical response of the CSF spaces subject to tapping.

Conclusions

We conducted an extensive parametric study of tracer dispersion in a subject-specific bench model of the human CNS which anatomical and functional reproduction of CSF dynamics from the spine to the cranium. A systematic variation of a parameters in large number of infusion experiments enabled in vitro quantification of the spatiotemporal tracer dispersion patterns and their dependence on significant infusion parameters and pulsatile CSF conditions. To the best of our knowledge, experimental data on the combined effect of infusion and natural oscillations have previously not been reported. Our experimental data underscore the possibility of targeting large sections of the neuroaxis or to the brain with the help of high-volume injection protocols. Infusion studies using human CSN models may serve as an inexpensive surrogate for testing and optimizing infusion protocols for the safe distribution of IT administered solutes along the neuraxis to inform clinical trials in humans.

Ethics approval and consent to participate

Not Applicable.

Availability of data and material

The details of all data are available in the appendixes, tables, and figures.

bioRxiv preprint doi: https://doi.org/10.1101/2022.03.22.485353; this version posted March 25, 2022. The copyright holder for this preprint (which was not certified by peer review) is the author/funder. All rights reserved. No reuse allowed without permission.

Competing interests

The authors declare that they have no competing interests.

Funding

National Science Foundation (https://www.nsf.gov), under grant number CBET-1301198.

National Institute of Health, Neurological Disorders and Stroke (https://www.ninds.nih.gov) under Grant number NIH NINDS 1R21NS099896. National Institute of Health, National Institute of Aging (https://www.nia.nih.gov) under grant NIH NIA 1R56AG066634-01.

Author details

[1]Department of Biomedical Engineering, University of Illinois at Chicago, Chicago, Illinois, USA. [2]Interning at UIC from EPF, Ecole D'Ingénieur, Paris, France. [3]Department of Neurosurgery, University of Illinois at Chicago, Chicago, Illinois, USA.

Acknowledgements

AL is grateful for funding from the National Science Foundation (https://www.nsf.gov), under grant number CBET-1301198. as well as the National Institute of Health, Neurological Disorders and Stroke (https://www.ninds.nih.gov) under Grant number NIH NINDS 1R21NS099896, and the National Institute of Aging (https://www.nia.nih.gov) under grant NIH NIA 1R56AG066634-01. We thank Dr. Gholampour at the University of Chicago for initial help with the statistical methods and figure editing.

bioRxiv preprint doi: https://doi.org/10.1101/2022.03.22.485353; this version posted March 25, 2022. The copyright holder for this preprint (which was not certified by peer review) is the author/funder. All rights reserved. No reuse allowed without permission.

References

[1] C. M. Bernards, "Cerebrospinal fluid and spinal cord distribution of baclofen and bupivacaine during slow intrathecal infusion in pigs," *Anesthesiology*, vol. 105, no. 1, pp. 169–178, 2006.

[2] R. M. Nelissen, Ed., *Fluid mechanics of intrathecal drug delivery*. Lausanne: EPFL, 2008. doi: 10.5075/epfl-thesis-4061.

[3] S. Tsangaris and N. Athanassiadis, "Diffusion in Oscillatory Flow in an Annular Pipe," *Angew. Math. U. Mech*, vol. 65, pp. T252–T254, 1985.

[4] J. Lee, A. Tripathi, and A. Chauhan, "Taylor dispersion in oscillatory flow in rectangular channels," *Chem. Eng. Sci.*, vol. 117, pp. 183–197, Sep. 2014, doi: 10.1016/j.ces.2014.06.022.

[5] K. Tangen, I. Nestorov, A. Verma, J. Sullivan, R. W. Holt, and A. A. Linninger, "In Vivo Intrathecal Tracer Dispersion in Cynomolgus Monkey Validates Wide Biodistribution Along Neuraxis," *IEEE Trans. Biomed. Eng.*, vol. 67, no. 4, pp. 1122–1132, Apr. 2020, doi: 10.1109/TBME.2019.2930451.

[6] S. Gholampour and M. Bahmani, "Hydrodynamic comparison of shunt and endoscopic third ventriculostomy in adult hydrocephalus using in vitro models and fluid-structure interaction simulation," *Comput. Methods Programs Biomed.*, vol. 204, p. 106049, Jun. 2021, doi: 10.1016/j.cmpb.2021.106049.

[7] L. Boussel *et al.*, "Phase-Contrast MRI measurements in intra-cranial aneurysms in-vivo of flow patterns, velocity fields and wall shear stress: A comparison with CFD," *Magn. Reson. Med. Off. J. Soc. Magn. Reson. Med. Soc. Magn. Reson. Med.*, vol. 61, no. 2, pp. 409–417, Feb. 2009, doi: 10.1002/mrm.21861.

[8] S. Bottan, D. Poulikakos, and V. Kurtcuoglu, "Phantom Model of Physiologic Intracranial Pressure and Cerebrospinal Fluid Dynamics," *IEEE Trans. Biomed. Eng.*, vol. 59, no. 6, pp. 1532–1538, Jun. 2012, doi: 10.1109/TBME.2012.2187448.

[9] K. Tangen, N. S. Narasimhan, K. Sierzega, T. Preden, A. Alaraj, and A. A. Linninger, "Clearance of Subarachnoid Hemorrhage from the Cerebrospinal Fluid in Computational and In Vitro Models," *Ann. Biomed. Eng.*, vol. 44, no. 12, pp. 3478–3494, Dec. 2016, doi: 10.1007/s10439-016-1681-8.

[10] S. J. Blundell and K. M. Blundell, *Concepts in Thermal Physics*. OUP Oxford, 2009.

[11] S. Basati, K. Tangen, Y. Hsu, H. Lin, D. Frim, and A. Linninger, "Impedance Changes Indicate Proximal Ventriculoperitoneal Shunt Obstruction In Vitro," *IEEE Trans. Biomed. Eng.*, vol. 62, no. 12, pp. 2787–2793, Dec. 2015, doi: 10.1109/TBME.2014.2335171.

[12] S. Basati, B. Desai, A. Alaraj, F. Charbel, and A. Linninger, "Cerebrospinal fluid volume measurements in hydrocephalic rats in: Journal of Neurosurgery: Pediatrics Volume 10 Issue 4 (2012) Journals." https://thejns.org/pediatrics/view/journals/j-neurosurg-pediatr/10/4/article-p347.xml (accessed Nov. 02, 2021).

[13] J. J. Lawrence *et al.*, "On the dispersion of a drug delivered intrathecally in the spinal canal," *J. Fluid Mech.*, vol. 861, pp. 679–720, Feb. 2019, doi: 10.1017/jfm.2018.937.

[14] K. M. Tangen, Y. Hsu, D. C. Zhu, and A. A. Linninger, "CNS wide simulation of flow resistance and drug transport due to spinal microanatomy," *J. Biomech.*, vol. 48, no. 10, pp. 2144–2154, Jul. 2015, doi: 10.1016/j.jbiomech.2015.02.018.

[15] N. Alperin, S. G. Hushek, S. H. Lee, A. Sivaramakrishnan, and T. Lichtor, "MRI study of cerebral blood flow and CSF flow dynamics in an upright posture: the effect of posture on the

bioRxiv preprint doi: https://doi.org/10.1101/2022.03.22.485353; this version posted March 25, 2022. The copyright holder for this preprint (which was not certified by peer review) is the author/funder. All rights reserved. No reuse allowed without permission.

intracranial compliance and pressure," in *Intracranial Pressure and Brain Monitoring XII*, Vienna, 2005, pp. 177–181. doi: 10.1007/3-211-32318-X_38.

[16] S. Birk, T. Geyer, R. Liedl, and M. Sauter, "Process-based interpretation of tracer tests in carbonate aquifers," *Groundwater*, vol. 43, no. 3, pp. 381–388, 2005, doi: 10.1111/j.1745-6584.2005.0033.x.

[17] S. Debnath, A. K. Saha, B. S. Mazumder, and A. K. Roy, "Transport of a reactive solute in a pulsatile non-Newtonian liquid flowing through an annular pipe," *J. Eng. Math.*, vol. 116, no. 1, pp. 1–22, Jun. 2019, doi: 10.1007/s10665-019-09999-1.

[18] K. k. Mondal and B. s. Mazumder, "On the solute dispersion in a pipe of annular cross-section with absorption boundary," *ZAMM - J. Appl. Math. Mech. Z. Für Angew. Math. Mech.*, vol. 85, no. 6, pp. 422–430, 2005, doi: 10.1002/zamm.200210180.

[19] P. Nagarani and B. T. sebastian, "Dispersion of a solute in pulsatile non-Newtonian fluid flow through a tube | SpringerLink," *Acta Mech*, vol. 224, pp. 571–585, 2013, doi: https://doi.org/10.1007/s00707-012-0753-6.

[20] P. M. Kaye *et al.*, "The immunopathology of experimental visceral leishmaniasis," *Immunol. Rev.*, vol. 201, no. 1, pp. 239–253, 2004, doi: 10.1111/j.0105-2896.2004.00188.x.

[21] J. W. Allen, K. A. Horais, N. A. Tozier, and T. L. Yaksh, "Opiate Pharmacology of Intrathecal Granulomas," *Anesthesiol. J. Am. Soc. Anesthesiol.*, vol. 105, no. 3, pp. 590–598, Sep. 2006.

[22] Y. B. Hsu, H. D. M. Hettiarachchi, D. C. Zhu, and A. A. Linninger, "The Frequency and Magnitude of Cerebrospinal Fluid Pulsations Influence Intrathecal Drug Distribution: Key Factors for Interpatient Variability. [Miscellaneous Article]," *Anesth. Analg. August 2012*, vol. 115, no. 2, pp. 386–394, 2012, doi: 10.1213/ANE.0b013e3182536211.

[23] Y. Hsu and A. A. Linninger, "Quantitative Integration of Biological, Pharmacokinetic, and Medical Imaging Data for Organ-Wide Dose-Response Predictions," *IEEE Trans. Biomed. Eng.*, vol. 60, no. 3, pp. 625–632, Mar. 2013, doi: 10.1109/TBME.2013.2244893.

[24] D. Banyte, M. Visbeck, T. Tanhua, T. Fischer, G. Krahmann, and J. Karstensen, "Lateral diffusivity from tracer release experiments in the tropical North Atlantic thermocline," *J. Geophys. Res. Oceans*, vol. 118, no. 5, pp. 2719–2733, 2013, doi: https://doi.org/10.1002/jgrc.20211.

[25] N. G. Barton, "On the method of moments for solute dispersion," *J. Fluid Mech.*, vol. 126, pp. 205–218, Jan. 1983, doi: 10.1017/S0022112083000117.

[26] R. Aris, "On the Dispersion of a Solute in Pulsating Flow Through a Tube," *Proceedings of the Royal Society of London. Series A, Mathematical and Physical Sciences*, vol. 259, pp. 370–376, Dec. 1960.

[27] L. Salerno, G. Cardillo, and C. Camporeale, "Aris-Taylor dispersion in the subarachnoid space," *Phys. Rev. Fluids*, vol. 5, no. 4, p. 043102, Apr. 2020, doi: 10.1103/PhysRevFluids.5.043102.

[28] A. L. Sánchez *et al.*, "On the bulk motion of the cerebrospinal fluid in the spinal canal," *J. Fluid Mech.*, vol. 841, pp. 203–227, Apr. 2018, doi: 10.1017/jfm.2018.67.

[29] E. J. Watson, "Diffusion in oscillatory pipe flow," *J. Fluid Mech.*, vol. 133, pp. 233–244, Aug. 1983, doi: 10.1017/S0022112083001883.

[30] G. I. Taylor, "Dispersion of soluble matter in solvent flowing slowly through a tube," *Proc. R. Soc. Lond. Ser. Math. Phys. Sci.*, vol. 219, no. 1137, pp. 186–203, Aug. 1953, doi: 10.1098/rspa.1953.0139.

bioRxiv preprint doi: https://doi.org/10.1101/2022.03.22.485353; this version posted March 25, 2022. The copyright holder for this preprint (which was not certified by peer review) is the author/funder. All rights reserved. No reuse allowed without permission.

[31] H. W. Stockman, "Effect of anatomical fine structure on the dispersion of solutes in the spinal subarachnoid space," *J. Biomech. Eng.*, vol. 129, no. 5, pp. 666–675, 2007, doi: 10.1115/1.2768112.

[32] K. M. Tangen, R. Leval, A. I. Mehta, and A. A. Linninger, "Computational and In Vitro Experimental Investigation of Intrathecal Drug Distribution: Parametric Study of the Effect of Injection Volume, Cerebrospinal Fluid Pulsatility, and Drug Uptake," *Anesth. Analg.*, vol. 124, no. 5, pp. 1686–1696, 2017, doi: 10.1213/ANE.0000000000002011.

[33] K. R. Hildebrand *et al.*, "Characterization of Effect of Repeated Bolus or Continuous Intrathecal Infusion of Morphine on Spinal Mass Formation in the Dog," *Neuromodulation Technol. Neural Interface*, vol. 22, no. 7, pp. 790–798, 2019, doi: 10.1111/ner.12963.

[34] H. C. W. Chu, S. Garoff, R. D. Tilton, and A. S. Khair, "Dispersion in steady and time-oscillatory flows through an eccentric annulus," *AIChE J.*, vol. 66, no. 2, p. e16831, Oct. 2019, doi: https://doi.org/10.1002/aic.16831.

[35] P. T. Haga *et al.*, "A numerical investigation of intrathecal isobaric drug dispersion within the cervical subarachnoid space," *PLOS ONE*, vol. 12, no. 3, p. e0173680, Mar. 2017, doi: 10.1371/journal.pone.0173680.

[36] F. Loth, M. A. Yardimci, and N. Alperin, "Hydrodynamic Modeling of Cerebrospinal Fluid Motion Within the Spinal Cavity," *J. Biomech. Eng.*, vol. 123, no. 1, pp. 71–79, Feb. 2001, doi: 10.1115/1.1336144.

[37] I. Venugopal, N. Habib, and A. Linninger, "Intrathecal magnetic drug targeting for localized delivery of therapeutics in the CNS," *Nanomed.*, vol. 12, no. 8, pp. 865–877, Apr. 2017, doi: 10.2217/nnm-2016-0418.

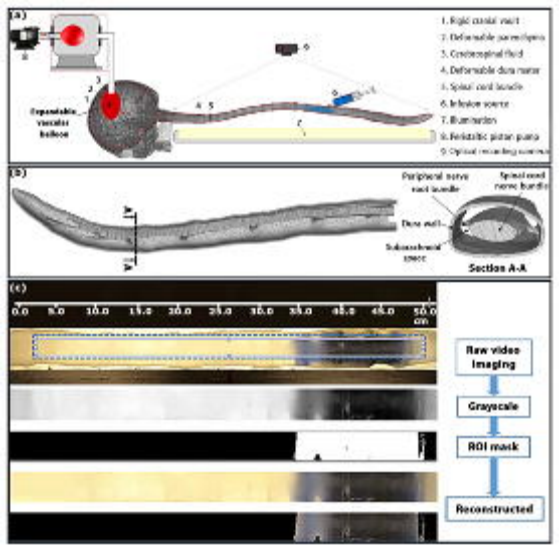
(a)
1. Rigid cranial vault
2. Deformable parenchyma
3. Cerebrospinal fluid
4. Deformable dura mater
5. Spinal cord bundle
6. Inflation source
7. Blunt tip
8. Pressure piston pump
9. Optical recording system
Expandable vascular bellows
(b)
Peripheral nerve root bundle
Spinal cord nerve bundle
Dura mall
Subarachnoid space
Section A-A
(c)
0.0 5.0 10.0 15.0 20.0 25.0 30.0 35.0 40.0 45.0 50.0 cm
Raw video imaging
Grayscale
ROI mask
Reconstructed

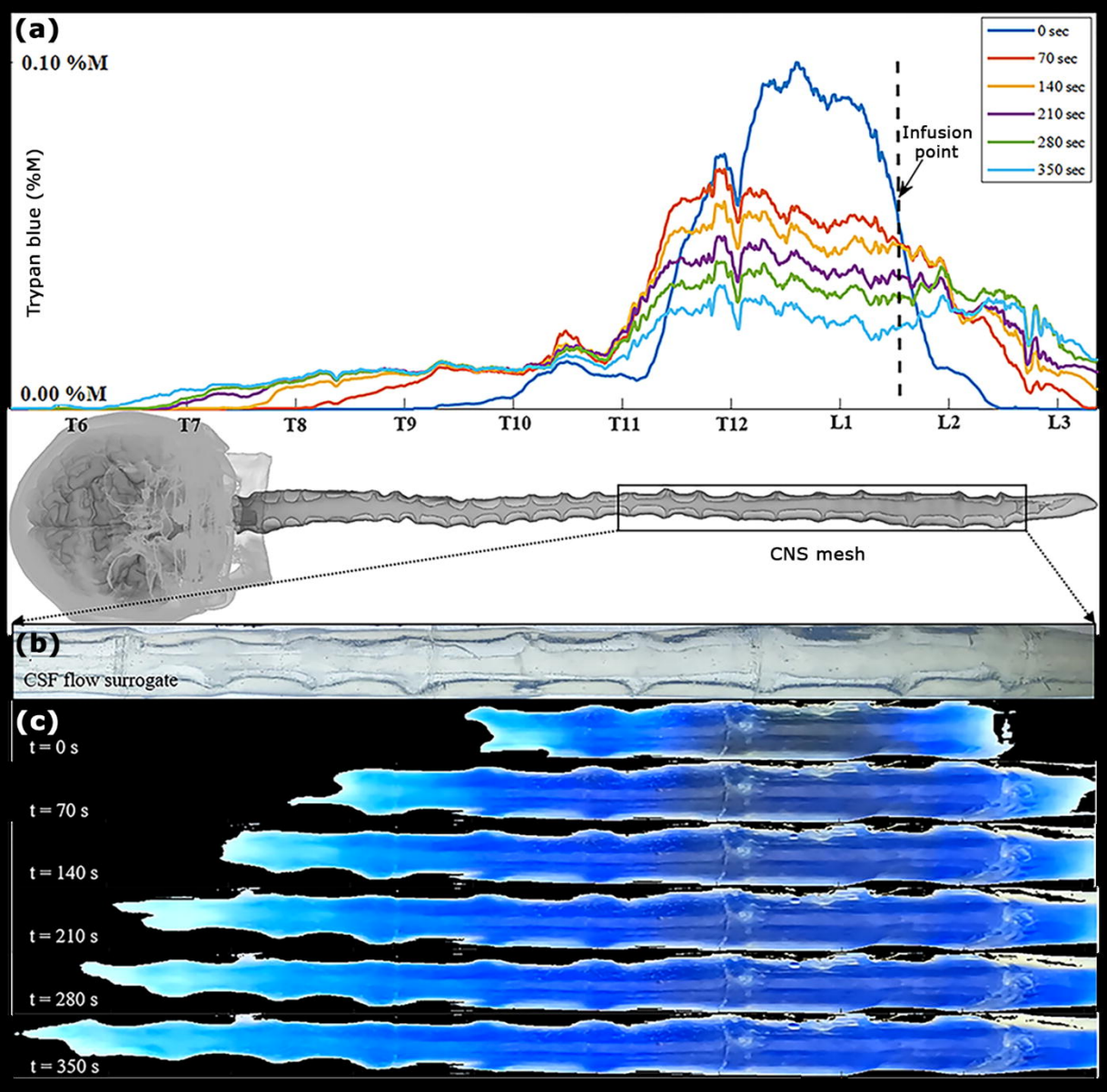
(a)
0.10 %M
Trypan blue (%M)
0.00 %M
0 sec
70 sec
140 sec
210 sec
280 sec
350 sec
Infusion point
T6
T7
T8
T9
T10
T11
T12
L1
L2
L3
CNS mesh
(b)
CSF flow surrogate
(c)
t = 0 s
t = 70 s
t = 140 s
t = 210 s
t = 280 s
t = 350 s

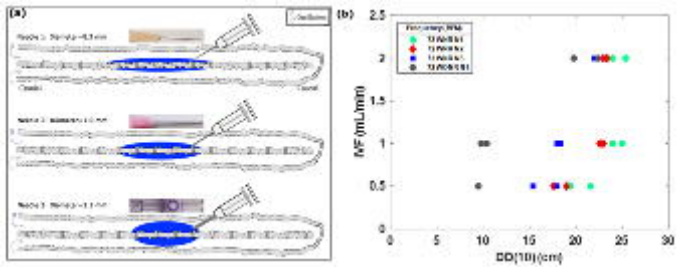
(a)
(b)
2.5
2
1.5
1
0.5
0
0
5
10
15
20
25
30
MF(mL/min)
DD(10)(cm)

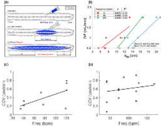
(A)
(B)
Frequency (bpm)
ZVF (mL/min)
(C)
CCV (cm/min)
Freq (bpm)
(D)
CCV (cm/min)
Freq (bpm)

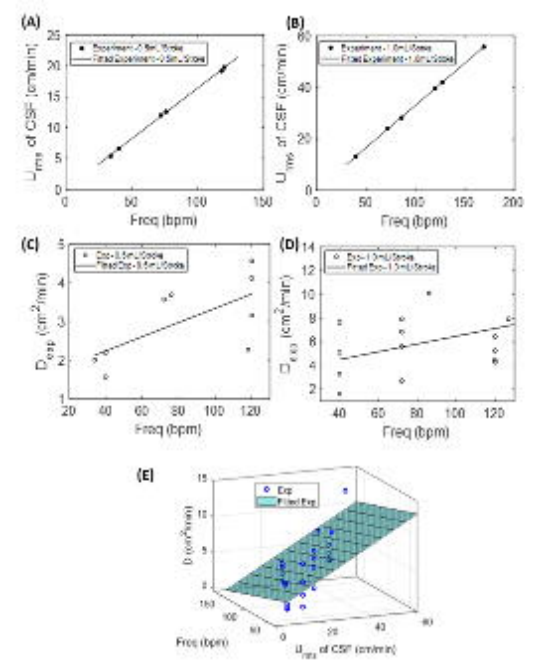
(A)
(B)
(C)
(D)
(E)
Freq (bpm)
Exp
Fitted Exp

(c)

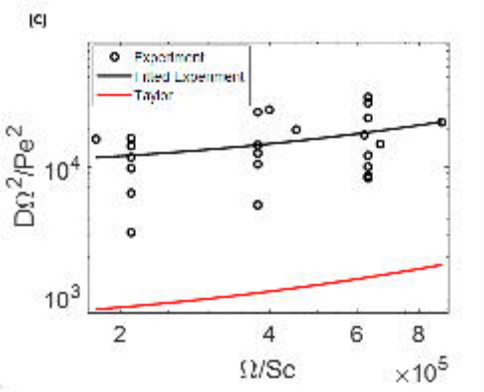
Experiment
Fitted Experiment
Taylor
$D\Omega^2/Pe^2$
10^4
10^3
2
4
6
8
Ω/Sc
$\times 10^5$

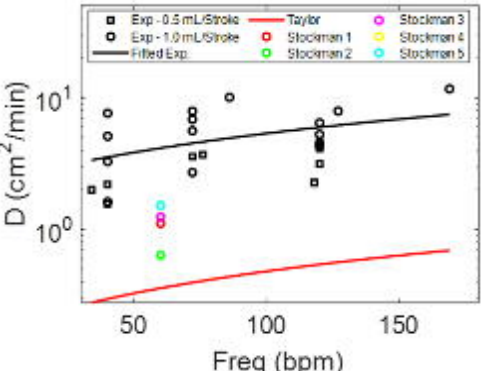
Exp - 0.5 mL/Stroke
Exp - 1.0 mL/Stroke
Fitted Exp.
Taylor
Stockman 1
Stockman 2
Stockman 3
Stockman 4
Stockman 5
D (cm2/min)
10^1
10^0
50
100
150
Freq (bpm)

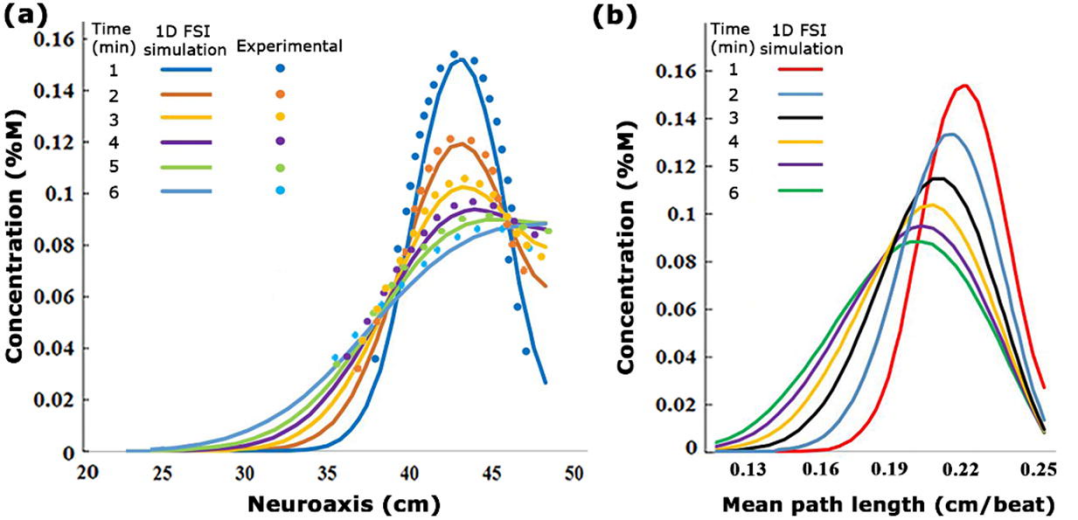
(a)
Time (min)
1D FSI simulation
Experimental
1
2
3
4
5
6
Concentration (%M)
0.16
0.14
0.12
0.1
0.08
0.06
0.04
0.02
0
20
25
30
35
40
45
50
Neuroaxis (cm)
(b)
Time (min)
1D FSI simulation
1
2
3
4
5
6
Concentration (%M)
0.16
0.14
0.12
0.1
0.08
0.06
0.04
0.02
0
0.13
0.16
0.19
0.22
0.25
Mean path length (cm/beat)